Journal of Advanced Ceramics
2015, **4**(1): 76–82
DOI: 10.1007/s40145-015-0136-2

ISSN 2226-4108
CN 10-1154/TQ

Research Article

Blister defect formation within partially stabilized zirconia film during constrained sintering

Kais HBAIEB[a,b,*]

[a]*Strategic Technology Unit*, *First Floor*, *Room G-08*, *Taibah University*, *P.O. Box 344*, *Al-Madinah Al-Munawwara*, *Kingdom of Saudi Arabia*
[b]*Mechanical Department*, *College of Engineering*, *Taibah University*, *P.O. Box 344*, *Al-Madinah Al-Munawwara*, *Kingdom of Saudi Arabia*

Received: September 16, 2014; Revised: November 10, 2014; Accepted: November 11, 2014

Abstract: Yttria stabilized zirconia (YSZ) film has been screen printed and sintered on a rigid substrate. The constrained sintering caused the formation of multiple microcracks and most critically large "blister" defects. The morphology of such defects has been characterized by scanning electron microscopy (SEM). It was revealed that the film surface exhibits noticeable roughness. Microhardness testing revealed little variation in green density distribution. Rheological measurement, however, showed that some agglomerations are present in the YSZ ink. The existence of agglomerations in the screen printing ink in combination with debonding at the film/substrate interface is potentially the cause for the formation of blister defects.

Keywords: constrained sintering; defects; yttria stabilized zirconia (YSZ); desintering; debonding

1 Introduction

Sintering of films is a necessary processing stage in many industrial applications. For example, in fabricating solid oxide fuel cell (SOFC) layer, anode, electrolyte and other layers have to be sintered together. Many technical difficulties may be encountered during sintering of these layers. In anode supported fuel cell, anode and electrolyte are co-sintered with the potential result of warpage if sintering is not well controlled [1,2]. In contrary, in substrate supported fuel cell, warpage is not possible as the substrate is usually thick and pre-sintered. However, constrained sintering of the electrolyte may result in defect formation and evolution that cause loss of leak tightness against gas flow through the electrolyte, a required condition for SOFC functionality.

Constrained sintering is a process in which the sintering of a ceramic body is slowed because of some constraint. Lange [3,4] reported that a phenomenon of desintering occurs concurrently with densification of powder compact when two particles forming necks undergo coarsening, constrained from sintering as a result of inclusions or pulled apart due to tension applied to the sintering body. When the green compact is not uniformly packed, the dense regions may act as hard inclusions in hindering the sintering of the surrounding matrix and desintering can also result. Although this phenomenon is observed in every sintered body, it is mostly obvious in layered structures when multiple layers are deposited onto a rigid substrate. Stresses arise either during sintering or upon cooling of the sintered structure. Because of sharp

* Corresponding author.
E-mail: hbaiebkais@gmail.com

transition of material properties, stress concentration can develop at the interface of adjoining layers. While sintering stress, which is the driving force for sintering, tends to cause the film to shrink, the substrate prevents the deformation; the densification completely stops parallel to the layers due to the bonding of layers but is free to take place normal to the layers (no constraint normal to the layers). Although the tensile stresses are not high in magnitude, they can trigger formation of fracture origins in the film as they develop in the very early stages where the particles have not bonded together, i.e., the film is weak [5–9]. Moreover, it is favorable for cracks to propagate further through the entire thickness of a constrained sintering film due to the high tangential sliding constraint that prevents particle rearrangement and induces large near crack tip stresses [10].

Anisotropic shrinkage in constrained sintering film has been observed in many studies [10–18]. Although this phenomenon is obvious in the presence of inclusions and inhomogeneous green density distribution within the pre-sintered film, it also arises when the film is uniformly deposited onto the substrate. Guillon *et al*. [13] showed anisotropic sintering develops in alumina film grown on a rigid substrate of the same material. Microstructure analysis of polished cross-sectional image in the thickness direction revealed preferential orientation of pores along the thickness direction. This anisotropy developed further as film density increased. Calata *et al.* [14] reported coarser pore distribution near the interface of a cordierite glass film with a rigid substrate as compared to the rest of the film. This was attributed to the constraint and poor wetting conditions at the film/substrate interface. Mohanram *et al.* [15] noticed higher pore density near the interface compared with the rest of the film material as the in-plane tensile stresses arisen from constrained sintering are higher at the film/substrate interface. Lu and Xiao [16] showed that relative density gradually increases as distance from interface increases to nearly reach a plateau far from the interface. In a recent paper, Martin and Bordia [17] used discrete element model to study the microstructure evolution of sintering film on a rigid substrate. They showed that constrained sintering at the interface causes large number of pores preferentially orienting themselves perpendicular to the substrate/ film planes and confirmed the observation of Lu and Xiao [16]. Martin and Bordia [17] also reported that the substrate does not negate the sintering dynamics of the particles but slows down the mobility of particles near the interface with some particle contacts growing at the expense of others.

In this paper, we discuss the effect of constrained sintering on the development of sintering defects within partially stabilized zirconia material screen printed and sintered on a rigid substrate.

2 Experimental procedure

Commercial 3 mol% yttria partially stabilized zirconia (YSZ, MEL chemicals, Manchester, UK) has been used for this study. The powder was mixed with terpinol based binder to produce a screen printing ink. The substrate used is pre-sintered porous magnesia-rich spinel substrate (Advanced Ceramics Ltd., UK). Prior to YSZ deposition, a porous layer of the same material (YSZ) with ~30 μm thickness was applied to the substrate to reduce roughness. In some cases, additional anode layer is printed to mimic the SOFC layer sequence. The ink was screen printed on a 40 mm × 40 mm printing area using screen printer (DEK Printing Machines Ltd., UK). In the printing process, a square blade was applied with a load of 12 kg on a stainless steel stencil with 165 mesh, with printing speed of 60 mm/s and 3 mm gap. For each sample, two consecutive printings (back and forth) were conducted. Once the printing was completed, the sample was dried at 120 ℃. The firing was conducted in a high-temperature furnace (Carbolite, UK) with a ramp rate of 2 ℃/min to 300 ℃, dwelled of 1 h and further heated to 1350 ℃ with a ramp rate of 3 ℃/min. The sintering temperature was hold for 1 h before cooling down to room temperature at a rate of 3 ℃/min. Selected samples were polished and gold coated for scanning electron microscopy (SEM) characterization.

Characterization for the samples for roughness and non-uniform green density distribution within the YSZ layer was also considered. Roughness of the zirconia film prior to sintering was measured using classical stylus profilometer. The density variation was studied by measuring microhardness across the electrolyte surface and relating hardness to density. The likelihood of density variation was thought to be due to either screen printing or presence of agglomerates within the YSZ ink. The latter hypothesis was also checked by further mixing the ink using ultrasonic processor. Viscosity and shear stress at various shearing rates of a stored ink and a fresh (ultrasonically) mixed ink were

measured using a rheometer (LAUDA Brinkmann, USA).

3 Results and discussion

As the YSZ film undergoes substantial shrinkage during sintering on a prefired substrate, residual tensile stresses arise and trigger formation of desintering defects. These typical defects seen in constrained sintering film have been reported in several studies and are shown in Fig. 1. It is believed that these defects are formed due to the tensile stresses developed during sintering due to the constraint applied by the substrate. As shown in Fig. 1, these defects prevent the electrolyte layer from reaching full density, but as long as they do not interlink or form a percolating network, the film may exhibit leak tightness against gas flow. A more critical type of defects has the form of a blister or volcano shape with large voids (several microns) that are very detrimental as they are permeable for gas flow. This was initially attributed to high internal pressure potentially due to the confinement of organic substances within the film; gases with increasing gas pressure (due to increase of temperature) eventually punch through the film causing such volcano type defect. However, this hypothesis is refuted for two reasons. First, organic binder shall be totally burned out at ~500 ℃ where the film is still porous and gas flow channels are abundant. Moreover, the film surface morphology for a film fired at 500 ℃ for 1 h has been recorded under SEM and is shown in Fig. 2(a). The absence of such defects is obvious; however, the micrograph reveals some unevenness of the surface profile. This has triggered the investigation of surface roughness evolution during printing and sintering process.

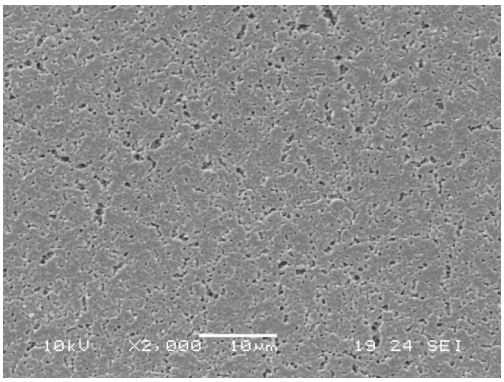

Fig. 1 Microcracks within electrolyte film due to constrained sintering.

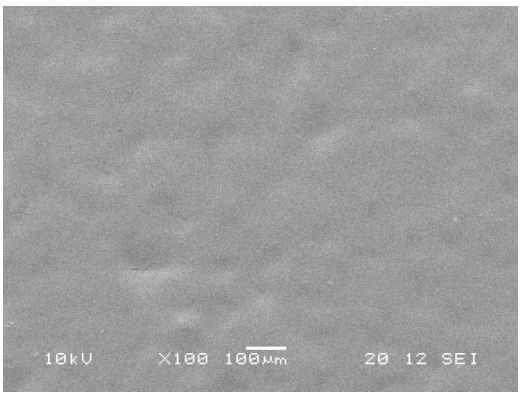

(a)

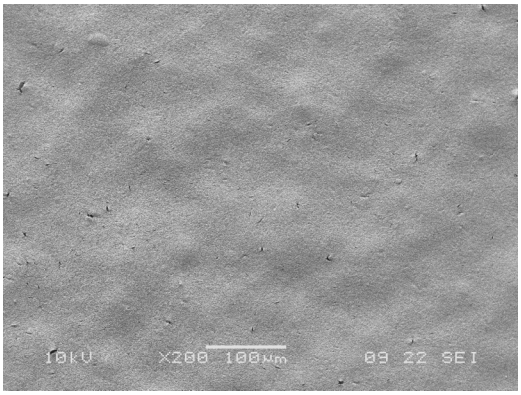

(b)

Fig. 2 Surface morphology of the electrolyte film: (a) fired at 500 ℃ for 1 h; (b) after complete sintering.

Roughness measurement of the substrate was conducted using classical stylus profilometer. Three measurements were conducted in extrusion and transversal directions. The roughness in the extrusion direction is usually higher than that in the transversal direction. The average roughness is ~4–4.5 μm. Three samples were used for these measurements. Porous zirconia thick film and anode were subsequently printed and co-sintered on the substrates (film thickness >40 μm). Roughness was again measured and the average roughness was ~3 μm. The YSZ electrolyte was then printed and the sample was fired at 1000 ℃ for 1 h (thickness ≈ 10 μm). Roughness was measured to be ~1.5 μm. Obviously the roughness reduces progressively as more films are deposited. The reduction in roughness is expected and easily conceptualized. Since roughness is an absolute quantity and sintering induces a thickness reduction irrespective of the original thickness, it is expected that the unevenness is reduced by the same shrinkage strain. That is, if the material is shrinking by 30% in the thickness direction, also shall the roughness reduce by the same amount. Note that a roughness of 1.5 μm is

considerable and may affect the sintering evolution within the film. It is interesting to note that roughness is quite noticeable after sintering as illustrated in Fig. 2(b). This could be the consequence of the original roughness but also potentially due to shrinkage differences that have taken place in the electrolyte film. That is, some regions within the film are shrinking by different amounts as compared to others. This non-uniformity of shrinking may be attributed to inhomogeneous green density distributions across the film.

The measurement of density variation across the electrolyte surface prior to sintering was more involved. It consists of hardness measurements not only at various locations on the electrolyte surface, but also on thin powder compacts made of electrolyte powder prepared using different compaction pressures to ensure different densities of the electrolyte powder compact. The hardness measurements of the thin powder compacts are necessary to correlate hardness to density. Weight and geometric dimensions were measured and density of the compacts was inferred. Hardness of powder compacts fired at 1000 ℃ for 1 h was measured at three locations (two opposite locations near the edge of the sample and one location at the center of the powder compacts). Dimensions before and after firing at 1000 ℃ were measured but shrinkage was infinitesimally small. The average of the hardness values for the different compacts was determined, and in combination of the density values a calibration curve was constructed that relates hardness to density (Fig. 3). In total five samples were prepared and we have used compaction pressure ranging from 1 ton to 5 tons with a 10 mm die. Higher pressure was not used to avoid cracking of the pellets. However, the calibration curve was fitted to a polynomial curve to extrapolate the densities beyond the measuring range when necessary. The hardness measurements were conducted using microhardness tester, where loads of 10 gf and 25 gf were applied. The samples were gold coated prior to hardness measurements for better clarity of the indentation shape.

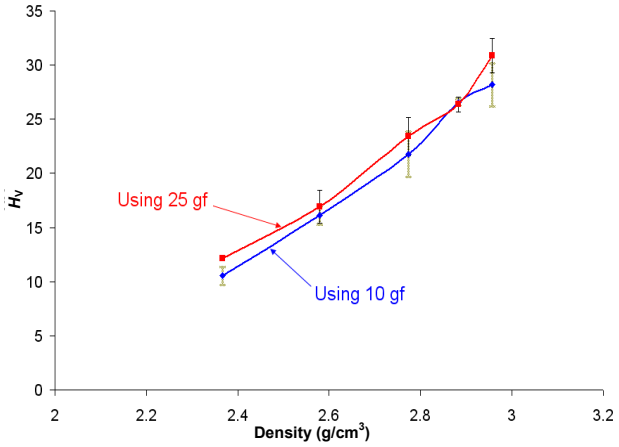

Fig. 3 Calibration curves relating hardness to density of powder compacts.

Microhardness across the electrolyte film surface fired at 1000 ℃ was measured at various locations spaced by 4 mm in the *x*- and *y*-directions and distributed throughout the entire surface. The load used for these measurements was the lowest, i.e., 10 gf (Fig. 4(a)). The density variation was then determined

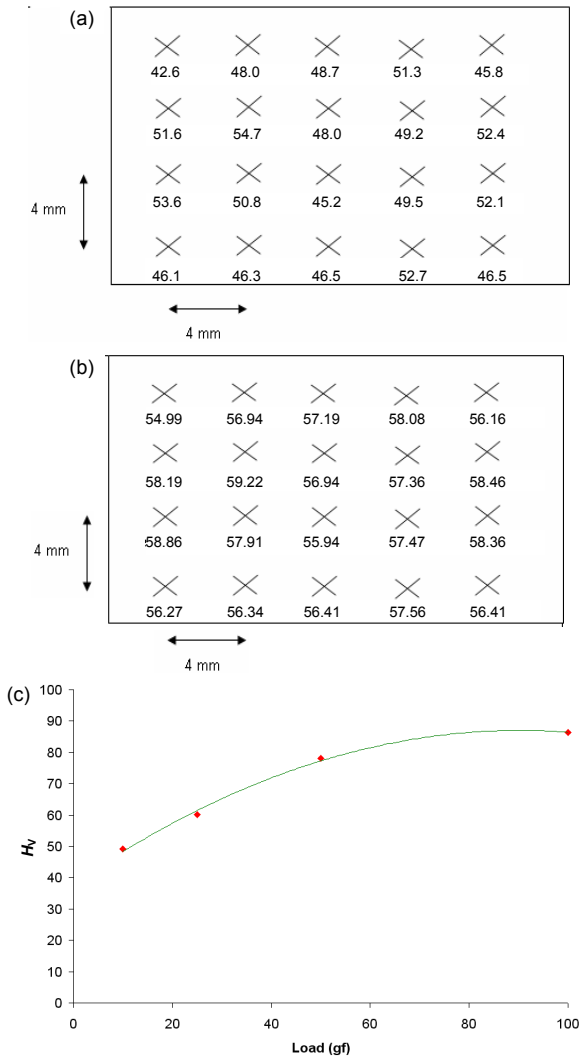

Fig. 4 (a) Microhardness results recorded at different locations across the *x*- and *y*-axes and using indentor load of 10 gf. (b) Density variation across the electrolyte surface determined using the measured microhardness results and the calibration curve. (c) Microhardness variation with the applied load. A plateau is reached at high indentor load which suggests that the hardness at high load is indeed the substrate hardness.

and given in Fig. 4(b). The geometrical in-plane dimensions measured were ~20 μm (dimensions of the indent imprint), which corresponds to a depth of ~8 μm. Obviously, this depth value is quite substantial relative to the electrolyte film thickness (~10 μm), and consequently the substrate underneath the electrolyte film must have influenced the measurements. This assertion was verified by conducting more hardness tests using higher loads and we have realized that the hardness increases to reach a plateau at high loads, up to 100 gf (Fig. 4(c)). It is believed that the hardness corresponding to high loads is no longer the hardness of the electrolyte but rather of the substrate. Using nanoindentation was not successful possibly due to the relatively large roughness (micron range). Despite the lengthy experimental duration, most of the measurements at different locations were not recorded. Referring to the most meaningful results using the lowest load of 10 gf, it seems that the density variation across the film is not large. Note that such analysis is not conclusive, not only because the substrate has affected the quantities measured, but also because the hardness is measured over a large film area (several microns) and hence only averaging values are determined.

The shelf life of a standard screen printing ink shall commonly extend for months. Ultrasonic processor was used for further mixing the electrolyte YSZ screen printing ink. Rheological characterization was conducted by measuring shear stress and viscosity versus shear rate. The results are shown in Fig. 5. As shown, both viscosity and shear stress have been reduced after ultrasonic processing which indicates the potential presence of agglomerations within the ink.

Figures 6(a), 6(b) and 6(c) illustrate three dimensional micrographs, showing several surface blister cracks, close-up of one defect and its cross-

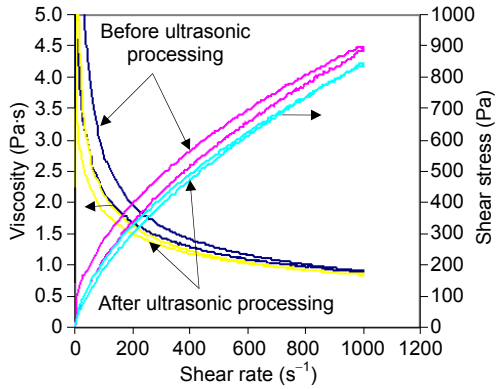

Fig. 5 Viscosity and shear stress versus shear rate before and after ultrasonic processing.

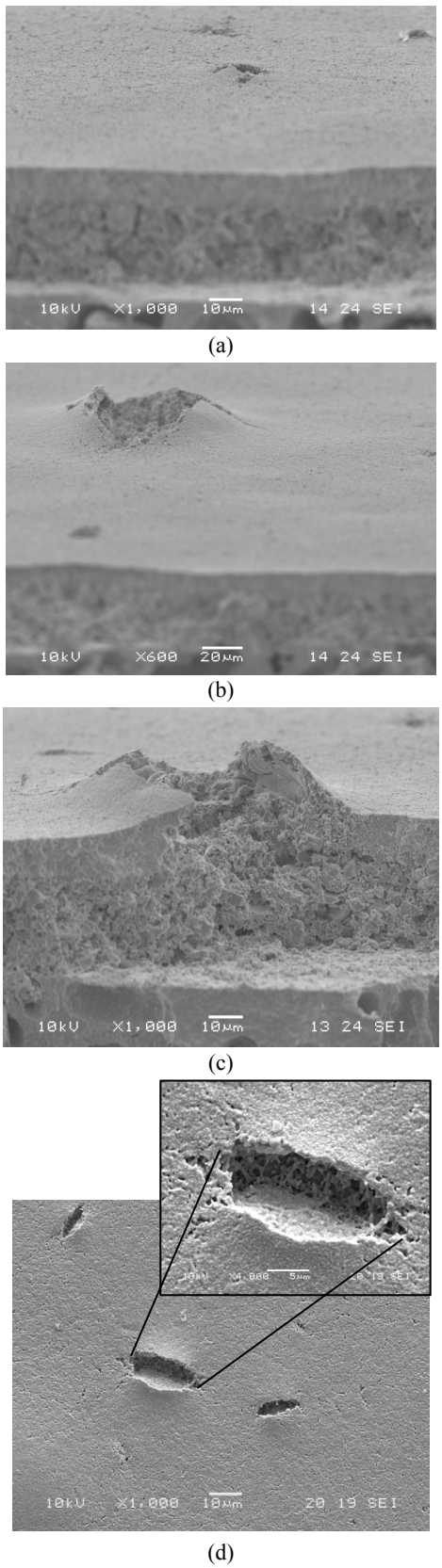

Fig. 6 (a) Several surface blister cracks, (b) close-up of one defect, (c) cross-sectional view of a blister defect and (d) one blister defect and its magnified shape extending much larger than 10 μm.

sectional view, respectively. Figure 6(d) shows one defect and its magnified shape extending much larger than 10 μm. Two smaller defects are randomly located in the proximity of the large crack. In general, these defects are randomly distributed and do not follow a defined pattern which contests the possibility of originating from screen printing mesh markings and reinforces the hypothesis that such defects are originated from low density regions that fail at the constrained sintering stress due to their poor initial packing. However, the blistering effect must be caused by a different phenomenon. Martin and Bordia [17] claimed that the dynamic of the sintering particles has an important effect on the microstructural evolution. The high viscous drag imposed by the substrate causes lack of mobility of particles at the film/substrate interface. Particles near the substrate do not sinter as much as those far from the substrate. The first few particle layers exhibit large porous microstructure with pores preferentially oriented along the thickness direction. The geometric and viscous drag imposed by the substrate causes several particle contacts to disappear for others to grow. When defects due to loss of particle contacts exceed critical size, such defects will grow further. This is manifested in local debonding of the film with the substrate. Henrich *et al.* [10] reported that once a defect is formed within a constrained sintering film it is readily to propagate through the thickness due to the presence of large near crack tip tensile stresses. The combination of surface cracking and debonding at the interface will create a free surface across the entire thickness. Free sintering in the near surface region will develop including curling that usually takes place in free standing film due to the in-plane sintering strains. The resulting shape resembles that of a blister or volcano shape protruding beyond the film surface level. We note that the porous structure is mostly developed at the substrate interface due to the high constraint applied by the substrate. Such constraint reduces as we go away from the interface. We speculate that the high sintering activity of the deposited film will accentuate such phenomenon at the film/substrate interface with the debonding and porosity density increasing. This is because the high sintering will intensify not only the densification process but also the growth of the large pores. In this particular study the YSZ film is very sintering active; dilatometry study showed that a powder compact sintered at 3 ℃/min to 1350 ℃ and hold for 1 h at the sintering temperature reaches full density with total engineering sintering strain of 27%. Such engineering strain corresponds to true strain of 32%. Tillman *et al.* [19] also reported that the sintering stress will gradually decrease as we go away from the interface to nearly disappear on the top surface. Hence, when a thick film is growing it is possible that the particles near the top surface will not feel any constraint from the substrate and behave as free sintering layer. Therefore, we recommend that graded layers shall be printed on the substrate with the low sintering active layer at the very bottom followed with gradual increasing sintering active layers. As such both debonding and surface crack may be eliminated or considerably reduced.

4 Conclusions

Yttria partially stabilized zirconia film has been screen printed and sintered on a rigid pre-sintered thick substrate. The constraint applied by the substrate resulted in formation of blister defects. The formation of such defects has been attributed to existence of agglomerations that have acted as fracture origins and to the high densification rate of the YSZ powders resulting in debonding at the interface.

References

[1] Li W, Hasinska K, Seabaugh M, *et al*. Curvature in solid oxide fuel cells. *J Power Sources* 2004, **138**: 145–155.

[2] Guo H, Iqbal G, Kang BS. Development of an *in situ* surface deformation and temperature measurement technique for a solid oxide fuel cell button cell. *Int J Appl Ceram Tec* 2010, **7**: 55–62.

[3] Lange FF. Densification of powder compacts: An unfinished story. *J Eur Ceram Soc* 2008, **28**: 1509–1516.

[4] Lange FF. De-sintering, a phenomenon concurrent with densification within powder compacts: A review. In *Sintering Technology*. German RM, Messing GL, Cornwall RG, Eds. New York: Marcel Dekker Inc., 1996: 1–12.

[5] Bordia RK, Raj R. Sintering behavior of ceramic films constrained by a rigid substrate. *J Am Ceram Soc* 1985, **68**: 287–292.

[6] Cheng T, Raj R. Flaw generation during constrained sintering of metal–ceramic and metal–glass multilayer

films. *J Am Ceram Soc* 1989, **72**: 1649–1655.
[7] Bordia RK, Jagota A. Crack growth and damage in constrained sintering films. *J Am Ceram Soc* 1993, **76**: 2475–2485.
[8] Wang X, Kim J-S, Atkinson A. Constrained sintering of 8 mol% Y_2O_3 stabilised zirconia films. *J Eur Ceram Soc* 2012, **32**: 4121–4128.
[9] Wang X, Atkinson A. Microstructure evolution in thin zirconia films: Experimental observation and modelling. *Acta Mater* 2011, **59**: 2514–2525.
[10] Henrich B, Wonisch A, Kraft T, *et al*. Simulations of the influence of rearrangement during sintering. *Acta Mater* 2007, **55**: 753–762.
[11] Fu Z, Dellert A, Lenhart M, *et al*. Effect of pore orientation on anisotropic shrinkage in tape-cast products. *J Eur Ceram Soc* 2014, **34**: 2483–2495.
[12] Heunisch A, Dellert A, Roosen A. Effect of powder, binder and process parameters on anisotropic shrinkage in tape cast ceramic products. *J Eur Ceram Soc* 2010, **30**: 3397–3406.
[13] Guillon O, Weiler L, Rödel J. Anisotropic microstructural development during the constrained sintering of dip-coated alumina thin films. *J Am Ceram Soc* 2007, **90**: 1394–1400.
[14] Calata JN, Matthys A, Lu G-Q. Constrained-film sintering of cordierite glass–ceramic on silicon substrate. *J Mater Res* 1998, **13**: 2334–2341.
[15] Mohanram A, Lee S-H, Messing GL, *et al*. Constrained sintering of low-temperature co-fired ceramics. *J Am Ceram Soc* 2006, **89**: 1923–1929.
[16] Lu X-J, Xiao P. Constrained sintering of YSZ/Al_2O_3 composite coatings on metal substrates produced from eletrophoretic deposition. *J Eur Ceram Soc* 2007, **27**: 2613–2621.
[17] Martin CL, Bordia RK. The effect of a substrate on the sintering of constrained films. *Acta Mater* 2009, **57**: 549–558.
[18] Green DJ, Guillon O, Rödel J. Constrained sintering: A delicate balance of scales. *J Eur Ceram Soc* 2008, **28**: 1451–1466.
[19] Tillman M, Yeomans JA, Dorey RA. The effect of a constraint on the sintering and stress development in alumina thick films. *Ceram Int* 2014, **40**: 9715–9721.